

Effects of long-wavelength fluctuations in large galaxy surveys

Anatoly Klypin^{1,2*} and Francisco Prada³

¹ *Astronomy Department, New Mexico State University, Las Cruces, NM, USA*

² *Department of Astronomy, University of Virginia, Charlottesville, VA, USA*

³ *Instituto de Astrofísica de Andalucía (CSIC), Glorieta de la Astronomía, E-18080 Granada, Spain*

7 August 2019

ABSTRACT

In order to capture as much information as possible large galaxy surveys have been increasing their volume and redshift depth. To face this challenge theory has responded by making cosmological simulations of huge computational volumes with equally increasing the number of dark matter particles and supercomputing resources. Thus, it is taken for granted that the ideal situation is when a single computational box encompasses the whole volume of the observational survey, e.g., $\sim 50 h^{-3} \text{Gpc}^3$ for the DESI and Euclid surveys. Here we study the effects of missing long-waves in a finite volume using several relevant statistics: the abundance of dark matter halos, the PDF, the correlation function and power spectrum, and covariance matrices. Finite volume effects can substantially modify the results if the computational volumes are less than $\sim (500 h^{-1} \text{Mpc})^3$. However, the effects become extremely small and practically can be ignored when the box-size exceeds $\sim 1 \text{Gpc}^3$. We find that the average power spectra of dark matter fluctuations show remarkable lack of dependence on the computational box-size with less than 0.1% differences between $1 h^{-1} \text{Gpc}$ and $4 h^{-1} \text{Gpc}$ boxes. No measurable differences are expected for the halo mass functions for these volumes. The covariance matrices are scaled trivially with volume, and small corrections due to super-sample modes can be added. We conclude that there is no need to make those extremely large simulations when a box-size of $1 - 1.5 h^{-1} \text{Gpc}$ is sufficient to fulfil most of the survey science requirements.

Key words: cosmology: Large scale structure - dark matter - galaxies: halos - methods: numerical

1 INTRODUCTION

Large-scale galaxy surveys such as the existing 2dFGRS (Hawkins et al. 2003), the SDSS (e.g., Anderson et al. 2012; Dawson et al. 2016), and the upcoming DESI (DESI Collaboration et al. 2016), Euclid (Laureijs et al. 2011), LSST (LSST Science Collaboration et al. 2009), and WFIRST (Spergel et al. 2013) are important for measuring cosmological parameters of our Universe, for studying the evolution of galaxies, and for unveiling the nature of dark matter and dark energy. In order to capture as much information as possible those survey observations have been increasing their volume and redshift depth. For example, the detection of the Baryonic Acoustic Oscillations (BAO) in the distribution of Luminous Red Galaxies (LRG) in the SDSS survey (Eisenstein et al. 2005) was based on 46,768 galaxies in a

volume $0.72 h^{-3} \text{Gpc}^3$. The BOSS measurements of cosmological parameters are based on 1.2 million LRGs in a volume of $5.8 h^{-3} \text{Gpc}^3$ (Alam et al. 2017). The volume of the DESI/Euclid and LSST surveys will be $\sim 50 h^{-3} \text{Gpc}^3$ and $\sim 100 h^{-3} \text{Gpc}^3$ respectively.

Theory has responded to this enormous survey volumes by making cosmological simulations of huge computational volumes with equally increasing the number of dark matter particles and the supercomputing resources. The Euclid Flagship Simulation, DarkSky and Outer Rim, with more than one trillion particles in a volume of $5-8 h^{-3} \text{Gpc}^3$ on a side, are good examples of the state-of-the-art achievements made recently in this field (Potter et al. 2017; Skillman et al. 2014; Habib et al. 2016).

Effects of computational box size were the topic of extensive discussions for the last few decades with introduction of different ideas and presentation of numerical results (e.g., Tormen & Bertschinger 1996; Cole 1997; Klypin et al. 1996;

* E-mail: aklypin@nmsu.edu

Table 1. Numerical and cosmological parameters of different simulations. The columns give the simulation identifier, the size of the simulated box in h^{-1} Mpc, the number of particles, the mass per simulation particle m_p in units of $h^{-1} M_\odot$, the mesh size N_g^3 , the gravitational softening length ϵ in units of h^{-1} Mpc, the number of time-steps N_s , the amplitude of perturbations σ_8 , and the number of realisations N_r . The last column gives references.

Simulation	Box	particles	m_p	N_g^3	ϵ	N_s	σ_8	N_r	Refs.
A0.5	500 ³	1200 ³	6.16×10^9	2400 ³	0.208	181	0.822	680	1
A1	960 ³	1200 ³	4.46×10^{10}	2400 ³	0.400	136	0.822	2532	1
A1.5	1500 ³	1200 ³	1.66×10^{11}	2400 ³	0.625	136	0.822	4513	1
A2.5	2500 ³	1000 ³	1.33×10^{12}	2000 ³	1.250	136	0.822	1960	1
A2.5c	2500 ³	1000 ³	1.33×10^{12}	2000 ³	1.250	285	0.822	1600	1
C1.2	1200 ³	1000 ³	1.47×10^{11}	3000 ³	0.400	136	0.822	100	3
D0.25	250 ³	1000 ³	1.33×10^9	2000 ³	0.125	181	0.822	120	3
D2.75	2750 ³	1100 ³	1.33×10^{12}	4400 ³	0.6250	136	0.822	22	3
D4	4000 ³	2000 ³	6.82×10^{11}	4000 ³	1.000	136	0.822	100	3
MDPL	1000 ³	3840 ³	1.5×10^9	–	0.010	–	0.828	1	2
HMDPL	4000 ³	3840 ³	7.9×10^{10}	–	0.025	–	0.828	1	2

References: ¹Klypin & Prada (2018), ²Klypin et al. (2016), ³this paper

Jenkins et al. 1998; Tinker et al. 2008; Angulo & White 2010; Klypin et al. 2016).

In the modern field of large cosmological simulations it is taken for granted that the ideal situation is when the volume of a single computational box covers the whole effective volume of the observational survey (e.g., Skillman et al. 2014; Comparat et al. 2017; Potter et al. 2017; Habib et al. 2016). But why is this true? It is clear why galaxy surveys must be large: we need to have as much information as possible, and the only way to do it is to increase the volume of the galaxy sample. However, what is the reason to have a single simulation box with a computational volume as large as possible? In the sense of statistics of matter density fluctuations (and related abundance of halos, voids, filaments and so on), one can produce as many realizations of the “universe” as needed in order to match the statistics seen in the observations. In terms of computational complexity (computational cost, access and dissemination of the results) we are in a more comfortable situation with many smaller simulation boxes. In any case we need to make many realizations to estimate noises and covariances – all needed for the data analysis of the surveys.

One can list a number of effects related with the finite volume of a simulation box. Those include the impact of periodically replicated images when a small computational box is replicated many times to mimic a large observational survey, and the effect of missing long-waves on the halo mass function, the clustering signal, and the covariance matrixes. Some of these effects have been already discussed in the literature (e.g., Hu & Kravtsov 2003; Warren et al. 2006; Skillman et al. 2014; Li et al. 2014b; Klypin & Prada 2018). Here we review the situation, and provide estimates and arguments, regarding the effects of long-waves in cosmological large-scale structure simulations.

The starting issue here is what observable one wants to study. If waves longer than ~ 1 Gpc are probed then there is no other option but to mimic those waves in theoretical estimates by using extreme computational volumes comparable to the size of the observable universe. Examples of these type of observables are the measurements of the power spectrum of fluctuations for wave-numbers $k \lesssim 0.001 h \text{Mpc}^{-1}$ or the two-point correlation function at $\sim 1 h^{-1} \text{Gpc}$ scale. In this case the computational volume must be extremely large.

However, in most of the cases the observables may not *explicitly* involve extremely long-waves. Consider as an example the abundance of very massive ($\gtrsim 10^{15} M_\odot$) clusters of galaxies. Clusters themselves have radii ~ 2 Mpc and gather mass from ~ 10 Mpc regions around them. So, the clusters are relatively small objects. However, their abundance depends *implicitly* on longer waves because those waves non-linearly couple with ~ 10 Mpc waves, which are responsible for the formation of the clusters. Another relevant example is the study of the Baryonic Acoustic Oscillations (BAO). The BAOs manifest themselves as a peak in the correlation function at pair separation of $\sim 100 h^{-1} \text{Mpc}$. Again, the signal of the peak is relatively small, but may *implicitly* depend on very long-waves through non-linear interactions.

The goal of this paper is to estimate the impact of missing long-waves in finite volume simulations on some important statistics that depend implicitly on those long waves.

This paper is structured as follows. We give a short introduction in Section 1. In Section 2 we present the suite of simulations used in this work. Methods and definitions are discussed in Section 3, and the impact of box replication is described in Section 4. The missing power estimates due to the lack of long-waves in the computational simulation box are given in Section 5, and the results of the impact on other statistics such as the correlation function, PDF, halo abundances, power spectrum and covariance matrix are presented on Sections 6, 7, 8 and 9. We study Super Scale Covariances (SSC) in Section 10. Finally we conclude and summarise our results in Section 11.

2 SIMULATIONS

Most of the results presented in this paper are based on cosmological N -body simulations. In Table 1 we present the numerical parameters of our simulation suite: box-size, number of particles, mass of a particle m_p , number of mesh points N_g^3 (if relevant), cell-size of the density/force mesh ϵ , the number of time-steps N_s , cosmological parameters σ_8 and Ω_m , and number of realizations N_r .

Different codes were used to make those simulations. The MultiDark Planck 1 $h^{-1} \text{Gpc}$ MDPL2 and 4 $h^{-1} \text{Gpc}$ HMDPL simulations (Klypin et al. 2016) were done with

the GADGET-2 code (Springel 2005). The other simulations were carried out with the parallel Particle-Mesh code GLAM (Klypin & Prada 2018). Because the GLAM code is much faster than GADGET-2, we have done many realisations of the simulations with the same cosmological and numerical parameters that only differ by initial random seed. All the GLAM simulations were started at initial redshift $z_{\text{init}} = 100$ using the Zeldovich approximation. These simulations span three orders of magnitude in mass resolution, a factor of hundred in force resolution, and differ by a factor of 10^5 in effective volume. The differences in box-size are large, which is important for analysis done in this paper, i.e., from $L = 250 h^{-1}\text{Mpc}$ to $L = 4 h^{-1}\text{Gpc}$. We did not study smaller boxes because simulations with $L \lesssim 250 h^{-1}\text{Mpc}$ become unpractical for large-scale structure studies even if finite box-size effects were corrected. They would also require too much replication to fill the observational volume. As we show below the box-size effects become too severe in those small boxes for relevant statistics such as the correlation function at the BAO peak and abundance of clusters of galaxies.

All simulations and analytical results presented in this work use the same cosmological parameters: a flat LCDM Planck cosmology with $\Omega_m = 0.307$, $h = 0.67$.

3 METHODS AND DEFINITIONS

A finite box-size L – either in simulations or in analytical estimates – yields an important parameter: the fundamental wavenumber, i.e.,

$$k_{\text{box}} = \frac{2\pi}{L}. \quad (1)$$

In order to estimate the matter power spectrum $P(k)$ from the GLAM simulations we generate the dark matter density field on a 3D-mesh of size N_g^3 (see Table 1). The Cloud-In-Cell (CIC) density assignment is used to estimate the density field. We then apply FFT to generate the amplitudes of N_g^3 Fourier harmonics. The minimum spacing of the harmonics in phase-space is $\Delta k = k_{\text{box}}$. The power spectrum is obtained on a 1D-mesh with constant binning equal to k_{box} . Each harmonic contributes to two mesh elements with the weights obtained using the CIC interpolation scheme in the same fashion as that used for the density assignment (Klypin & Prada 2018). This binning procedure reduces the noise in the power spectrum by $\sim 30\%$. The power spectrum is corrected for the aliasing due to the CIC density assignment.

The covariance matrix $C(k, k')$ of the power spectrum is defined as a reduced cross product of the power spectra at different wave-numbers k and k' for the same realisation averaged over different realisations:

$$C(k, k') = \langle P(k)P(k') \rangle - \langle P(k) \rangle \langle P(k') \rangle. \quad (2)$$

The covariance matrix is typically normalized by the average amplitude of the diagonal components and plotted as $[C(k, k')/P(k)P(k')]^{1/2}$.

When estimating the density distribution function (PDF) for a given simulation we use a different 3D-mesh size N not necessarily equal to the mesh size of the simulation itself. The CIC density scheme is applied for every mesh

size used. Once the overdensity field is created the values of the overdensity $\rho = \rho_{\text{DM}}/\langle \rho_{\text{DM}} \rangle$ are binned using logarithmically spaced bins with width $\Delta \log_{10}(\rho) = 0.025 - 0.050$. The PDF is then defined as a normalized number ΔN of cells with overdensity in the range $[\rho, \rho + \Delta\rho]$, i. e.,

$$P(\rho) = \frac{\Delta N}{N^3 \Delta \rho}. \quad (3)$$

By construction, the PDF is normalized to have the total volume and the total mass density to unity. The second moment of $P(\rho)$ is the *rms* fluctuation of the overdensity field and is related to the power spectrum of fluctuations in simulations by

$$\sigma^2 = \int_0^\infty (\rho - 1)^2 P(\rho) d\rho = \frac{1}{2\pi^2} \int_{k_{\text{box}}}^{k_{\text{Ny}}} P(k) W^2(k\Delta x) k^2 dk, \quad (4)$$

where $\Delta x = L/N$ is the cell-size of the density field and $k_{\text{Ny}} = \pi/\Delta x$ is the Nyquist frequency of the mesh. Here $W^2(k\Delta x)$ is the power spectrum of the CIC filter with cell size Δx .

Depending on the cell size the PDF can have a very wide range of values. For the relatively small cell-sizes $\Delta x = (1 - 5) h^{-1}\text{Mpc}$ used in this paper the leading term in the PDF is $P(\rho) \propto \rho^{-2}$ (Bouchet et al. 1991; Klypin et al. 2017). In order to reduce the dynamical range of the PDF we typically plot $\rho^2 P(\rho)$.

4 EFFECTS OF BOX REPLICATIONS

If the computational box of the simulation is smaller than the volume of a given galaxy survey, **the same** simulation box must be replicated enough times to cover the entire observed region. Note that in order to avoid defects at the boundaries of the box, the same realization is replicated. Box replications increase the apparent volume of the sample as compared to the volume of a single simulation. However, they do not add new information: it is still the same as in the original simulation. For example, if long-waves were absent in the simulation box, they will be absent in the replications. Nothing wrong with this: it is understood that something will be missing if the replication is applied to a finite volume simulation. The main question is: will the replication procedure produce any defects?

One can imagine some possible issues. We start with the obvious one: the same structure will be observed again and again due to the periodical replication. Figure 1 illustrates the situation. Here we use halos drawn from the MDPL ($1 h^{-1}\text{Gpc}$) and HMDPL ($4 h^{-1}\text{Gpc}$) simulations with virial masses larger than $M > 10^{14} h^{-1} M_\odot$. We assume that in this case the observational “sample” has a depth of $2000 h^{-1}\text{Mpc}$ and we also show halos in a somewhat arbitrary chosen (but large) $400 h^{-1}\text{Mpc}$ slice. The bottom panel shows halos selected from the much larger HMDPL simulation. No replication is needed in this case because the HMDPL simulation covers the whole “observed” volume. The situation is different in the case of the $1 h^{-1}\text{Gpc}$ MDPL simulation that requires 8 replications: 4 times along the x-axis and two along the y-axis. Indeed one clearly sees the effects of the replications (see top panel in Figure 1). This is obviously not a pleasant feature: the real universe should not look like that. However, is it really a problem? Once we agreed (or found)

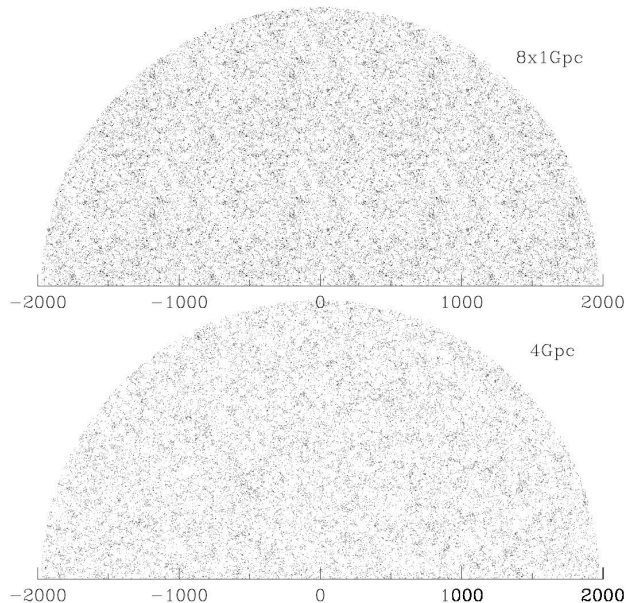


Figure 1. Distribution of dark matter halos with mass $M > 10^{14} h^{-1} M_{\odot}$ in a $400 h^{-1} \text{Mpc}$ slice with distances $R < 2000 h^{-1} \text{Mpc}$. The horizontal axis shows scales in $h^{-1} \text{Mpc}$ units. The bottom panel shows the sample distribution for the HMDPL simulation with a computational box of $4 h^{-1} \text{Gpc}$ on a side. No replication was done in this case. The top panel is for the MDPL simulation with a computational box of $1 h^{-1} \text{Gpc}$ on a side. In this case the halo sample was periodically replicated many times to cover the same coordinate domain. This replication leads to repeating images of the same structures that can be seen more clearly in the central region of the plot.

that waves longer than the computational box are not important, then there is nothing wrong with the top panel in Figure 1. What we perceive as a defect in the plot is just a way for our brain to tell us that there are no waves longer than $1 h^{-1} \text{Gpc}$. Indeed, if we had analysed the new (replicated) sample and ignored the effects of sample boundaries, we would have found the same properties as in the original small volume simulation – the same halo abundances, peculiar velocities, correlation function, and the same power spectrum truncated at the fundamental mode of the simulation box.

There is a simple way to remedy the visual problems with the replications. One needs to rotate the stacked simulations before making mock observational samples: the same realization is stacked and the resulting distribution is rotated. We illustrate this by rotating twice the stacked distribution of halos in the $1 h^{-1} \text{Gpc}$ MDPL simulation. We first rotate by some angle ($\sim 30^{\circ} - 60^{\circ}$) the distribution along the y-axis (the vertical axis in Figure 1), and then by another angle along the x-axis (horizontal axis in the same plot). After the rotations are done, we make the same slice as described before. Figure 2 shows two examples of mock samples produced in this way. The plots do not show any visual defects of the replications. Just as in the case of a simple replication, the rotated stacked distribution does not bring new information. For example, if we estimate the

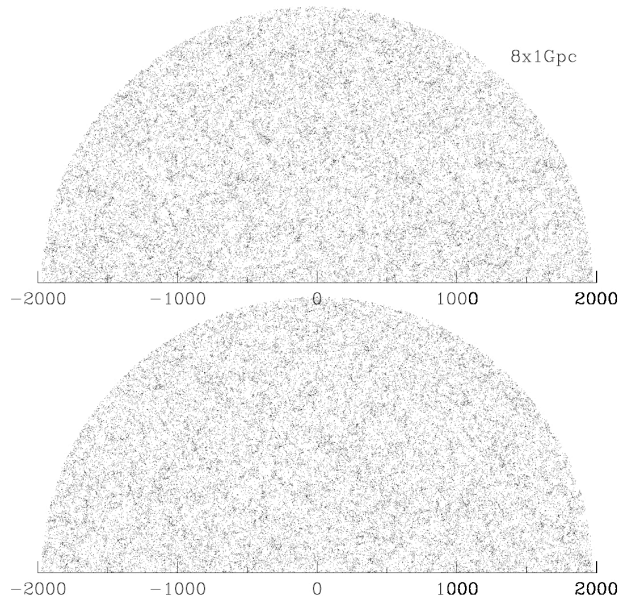


Figure 2. The same as in Figure 1, but with the computational volume of the $1 h^{-1} \text{Gpc}$ MDPL simulation replicated and rotated along the x- and y- axes. The top and bottom panels are for two different rotation angles (see text). No periodical structures are seen in these images.

power spectrum of fluctuations of the rotated and stacked distribution, we will find the same power spectrum as that found in the original $1 h^{-1} \text{Gpc}$ box with shifted angles of the harmonics.

The other potential issue with the replication process is repeating structures (halos, voids, filaments) along the line-of-sight. An example is the study of the weak-lensing signal produced by clusters of galaxies or individual galaxies. In order to mimic observations, the same simulation can be repeated many times (stacked) along the line-of-sight with an “observer” placed on the line going through the centres of the aligned boxes. If the box is small and the observer is at a large distance from the lens, then every object will be found replicated many times along the line-of-sight, which constitutes a serious defect for the weak-lensing estimates.

The key issue here is the size of the simulation. If it is too small, say $100\text{--}200 \text{Mpc}$, then indeed the replication is problematic. With the typical distance to lenses of $\sim 1 h^{-1} \text{Gpc}$ a small $\sim 100 h^{-1} \text{Mpc}$ box will result in almost plane-parallel projection on the sky and, thus, with multiple halos almost exactly along the line-of-sight. The situation is different for large simulations with size $\sim 1 h^{-1} \text{Gpc}$. In this case multiple replications are still required, but they do not produce problems for weak-lensing estimates. Figure 3 schematically illustrates this situation with the replications of a large computational box. To make the problem more transparent we place four objects in a 2D-box of unit size and replicate it 3 times in each direction. The “observer” is placed in the corner of the box and the lines connecting the observer going through each point are shown. Most of the lines do not have periodical images. The only one that does

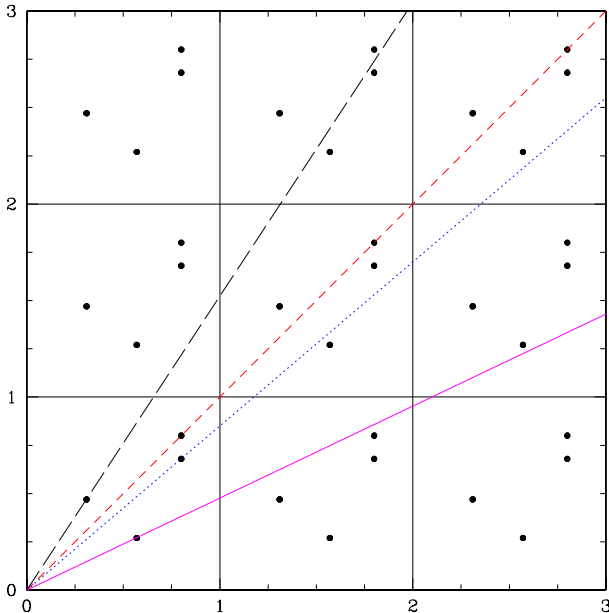


Figure 3. Illustration of the effects of replication of a large simulation box. Four objects were placed in a square of size one and then replicated 3 times along the x-axis and three times along y-axis. The observer is placed in the left bottom corner of the resulting 3×3 square. The line-of-sight periodically replicated images that present a problem for the weak-lensing analysis are only for those objects along the diagonal of the square and its main axes, which are highly improbable configurations.

is the object that is exactly along the diagonal. We know which points will have periodical images and which, thus, will have problems with lensing analysis. If (x, y) are the coordinates of the objects, then periodical images will appear if the ratio of the coordinates is a rational number. In other words, if $x/y = i/j$; where i, j are integer numbers. A periodical image appears after i replications along the x-axis and j replications along the y-axis. Because we replicate the simulation box only few times (three for Figure 3), we are potentially interested in the cases with small values of i and j . In a mathematical sense the probability of an arbitrary x and y to be a rational number is zero. In 3D the situation is even more strict because two ratios x/y and y/z must be rational with small integers. In practice the chance to have close images along the line-of-sight of the same object are very small and can be found in every case.

5 MISSING POWER

The size of the computational volume defines another important ingredient: the amplitude of the power missed in the simulation box. The larger is the box the smaller is the missing power and, thus, the simulation closely matches the density fluctuations in the Universe. We can estimate the missing power σ_{miss} by integrating the linear power spectrum $P(k)$ from $k = 0$ up to the wavenumber given by the

fundamental mode of the box k_{box} , i.e.,

$$\sigma_{\text{miss}}^2(L) = \frac{1}{2\pi^2} \int_0^{k_{\text{box}}} P(k)k^2 dk, \quad k_{\text{box}} = 2\pi/L. \quad (5)$$

The missing power can be computed for any redshift, but here we will do the estimates only for $z = 0$. The bottom panel in Figure 4 shows $\sigma_{\text{miss}}(L)$ for different box-sizes L .

The plot shows that the missing power declines dramatically with increasing box-size. This is expected because at small k the power spectrum $P(k)$ is nearly primordial with slope ~ 1 . Thus, $\sigma^2 \propto k^4 \propto L^{-4}$. While it is easy to estimate $\sigma_{\text{miss}}(L)$ numerically, it is convenient to have a simple approximation for large simulation boxes and Planck cosmology:

$$\sigma_{\text{miss}}(L) \approx \frac{7.5 \times 10^{-3}}{L_{\text{Gpc}}^2}, \quad L_{\text{Gpc}} \equiv \frac{L}{1 h^{-1} \text{Gpc}}. \quad (6)$$

The other side of this steep decline is that the missing power *increases* dramatically for small boxes. For example, for $L = 200 h^{-1} \text{Mpc}$ the missing power is $\sigma_{\text{miss}} \approx 0.1$, which is substantial considering that one expects that non-linear effects (e.g., turn-around for halo formation) become important when the overdensity becomes unity. However, the missing power becomes very small, and falls below $\sigma_{\text{miss}} < 10^{-2}$, for a $L = 1 h^{-1} \text{Gpc}$ simulation box.

There are different ways of assessing how large is the power missed in a finite box size. The other lines in the bottom panel of Figure 4 correspond to the power in eq.(5) integrated up to a giving wavenumber k_{cut} instead of k_{box} . We use two values of k_{cut} : $0.1 h \text{Mpc}^{-1}$ and $0.3 h \text{Mpc}^{-1}$ which are characteristic for the domain of the BAO peaks. The full curves are for the total power (infinite box) and the dashed curves are for the power inside the box (with the integrals starting at k_{box}). Clearly there is not much missing power except for those boxes with $L \lesssim 200 h^{-1} \text{Mpc}$. The top panel in Figure 4 shows the ratio of missing power in waves with $k < k_{\text{box}}$ to the power inside the specified wavenumber indicated in the plot. The missing *rms* power can be substantial for simulations with boxes smaller than $\sim 200 h^{-1} \text{Mpc}$, but it becomes tiny for simulations with boxes larger than $\sim 1 h^{-1} \text{Gpc}$.

It is also interesting to note that most of the missing power $\sigma_{\text{miss}}(L)$ is found in waves that are just a bit longer than the computational box. For example, for a $1 h^{-1} \text{Gpc}$ box 95% of the missing power is in waves with wavelengths between $(1 - 2) h^{-1} \text{Gpc}$ and 88% is in $(1 - 1.5) h^{-1} \text{Gpc}$ waves. These waves cannot be considered constant inside the computational box: a striking contrast with the main presumption of the separate universe simulations (e.g., Li et al. 2014b; Wagner et al. 2015) which assumes that the only long-waves that matter are those that are much longer than the length of the computational box, and, thus, can be treated as a constant background. The *rms* density fluctuation σ_L of the average density inside a box L embedded in an infinite density field is about 5 times smaller than $\sigma_{\text{miss}}(L)$. See Section 11 for more details.

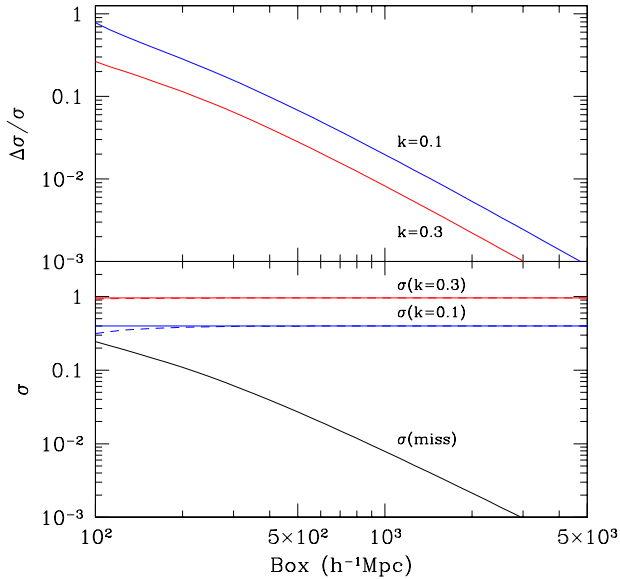


Figure 4. Missing dark matter power of density fluctuations in simulations with different box sizes. *Bottom panel:* The lower full curve shows the *rms* of density fluctuations in waves longer than the box-size $k < k_{\text{box}} = 2\pi/L$. The other curves show the *rms* fluctuations up to $k = 0.1h\text{Mpc}^{-1}$ (lower curves) and $k = 0.3h\text{Mpc}^{-1}$ (top curves): the full curves show the total *rms* including waves up to the distance to the horizon while the dashed curves are for waves from the box size down to the specified wavenumber. *Top panel* shows the ratio of the missing power in waves with $k < k_{\text{box}} = 2\pi/L$ to the power inside the specified wavenumber indicated in the plot. The missing *rms* power can be substantial for simulations with boxes smaller than $\sim 200 h^{-1}\text{Mpc}$. It becomes tiny for simulations with boxes larger than $\sim 1 h^{-1}\text{Gpc}$ where most of the missing power is in waves that are just a bit longer than the box-size.

6 IMPACT ON THE CORRELATION FUNCTION

Because of the truncation of the power spectrum at the fundamental mode, the finite-size box correlation function of the dark matter is different at large scales from that expected when one assumes an infinite volume (Sirko 2005; Klypin et al. 2013). The correlation function of the dark matter or that of halos are affected by non-linear processes. Still, their main features (e. g., position of the BAO peak and zero-crossing; see Figure 5 in Klypin et al. (2013)) are reproduced by the linear theory with some modifications though. In any case, it is important to estimate how accurately we can even reproduce the linear correlation function.

The finite box-size correlation function $\xi(R)$ can be estimated using the power spectrum $P(k)$, i. e.,

$$\xi(R) = \frac{1}{2\pi^2} \int_{k_{\text{box}}}^{\infty} dk k^2 P(k) \frac{\sin(kR)}{kR}. \quad (7)$$

Figure 5 presents the estimates of the correlation function of the linear dark matter power spectrum for different box-sizes. Just as expected, the differences become small at smaller scales. Indeed, the comparison of the correlation functions of halos in the Bolshoi ($L = 250 h^{-1}\text{Mpc}$) and

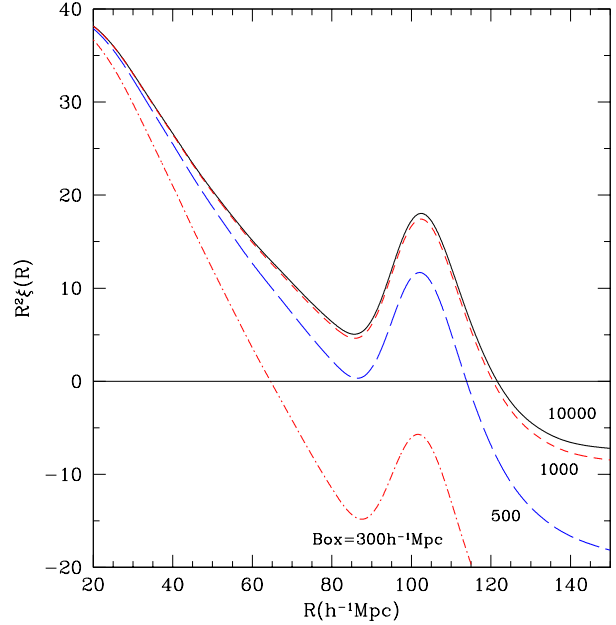


Figure 5. Effects of the box-size on the correlation function $\xi(R)$ in the linear regime. We estimate the correlation function using the linear power spectrum truncated on wavenumbers smaller than the fundamental mode, $k < k_{\text{box}}$, with the box-size indicated in the plot. The peak of ξ at $R_{\text{BAO}} \approx 100 h^{-1}\text{Mpc}$ is due to the BAO. For larger box-sizes the correlation function crosses zero at $R_0 \approx 122 h^{-1}\text{Mpc}$. When the box-size becomes small the amplitude of the correlation function decreases at large radii: the zero-crossing shifts to much smaller distances and the BAO amplitude is severely affected.

MultiDark ($L = 1 h^{-1}\text{Gpc}$) simulations are also within few percent for $R < 10 h^{-1}\text{Mpc}$ (Klypin et al. 2013).

At larger scales the box-size effects become more apparent. For example, for a $L = 300 h^{-1}\text{Mpc}$ box the correlation function is qualitatively incorrect: the whole BAO domain is negative and the zero-crossing scale is twice smaller than it should be (see Figure 5). The situation improves when the box-size increases. However, the box-size should be substantially larger than $500 h^{-1}\text{Mpc}$ in order to closely match the correlation function of the infinite box.

Just as with the estimates of the missing power, the effects due to the missing long-waves dramatically decline with increasing of the box size. Indeed, we can hardly see any impact for $L = 1 h^{-1}\text{Gpc}$. We can quantify the effect using two statistics: the position of the BAO peak R_{BAO} and the scale of zero-crossing R_0 . These two parameters are plotted in Figure 6. As we can see, the position of the BAO is remarkably stable. For the $L = 500 h^{-1}\text{Mpc}$ box the BAO peak is within 0.1% from its pristine location, and the deviations become unmeasurable for larger boxes. This is good news because the BAO position is an important parameter for estimates of the cosmological parameters. It will be modified by non-linear effects, but at least we start with an accurate linear theory position.

The zero-crossing is much more sensitive to the box-size with large uncertainties for boxes with $L < 500 h^{-1}\text{Mpc}$.

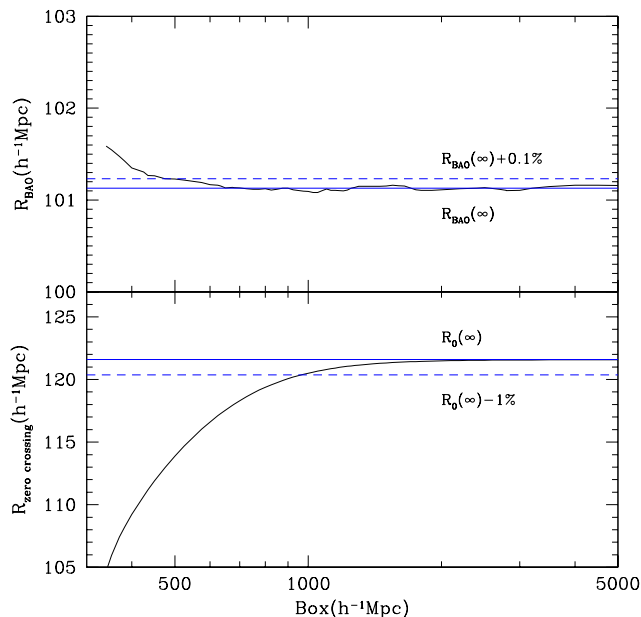


Figure 6. Dependence of the BAO peak R_{BAO} (top panel) and the zero-crossing R_0 (bottom panel) on the box-size in the linear correlation function. The position of the BAO peak is very insensitive to the box-size with 0.1% change for a box with $L \approx 500 h^{-1}\text{Mpc}$. The zero-crossing R_0 is much more affected: for better than 1% error the simulation box must be larger than $1 h^{-1}\text{Gpc}$.

Still, the error decreases quickly with increasing the box-size, and becomes less than 1% for $L > 1 h^{-1}\text{Gpc}$.

We study also the effects of nonlinear evolution using the C1.2 and D2.75 GLAM simulations at $z = 0$. Figure 7 presents the average correlation function of dark matter in these simulations for a wide range of radii $R = (1 - 150) h^{-1}\text{Mpc}$. If the long-waves missed in the C1.2 simulation boxes, as compared with the much larger boxes of the D2.75 simulations were important, we would have seen a stronger clustering in $2.75 h^{-1}\text{Gpc}$ box simulations at all scales. However, this does not happen: there are no measurable differences between the $1.2 h^{-1}\text{Gpc}$ and the much larger $2.75 h^{-1}\text{Gpc}$ simulations for scales $R > 5 h^{-1}\text{Mpc}$.

In order to quantify the differences in the BAO domain, we fit the average correlation functions of each set of simulations with an analytical function – a third order polynomial in the form:

$$\xi_{\text{fit}}(R) = \xi_0 + a_1 x + a_2 x^2 + a_3 x^3, \quad x \equiv R - R_0. \quad (8)$$

The function has 5 free parameters with R_0 and ξ_0 defining the position and amplitude of the peak of the correlation function. After fitting the data in the range of radii $R = (91 - 113) h^{-1}\text{Mpc}$ we find for $L = 2.75 h^{-1}\text{Gpc}$ simulations $\xi_0 = 1.500$, $R_0 = 100.30 h^{-1}\text{Mpc}$, which is nearly identical (within 0.06% for R_0) with those for the C1.2 simulations: $\xi_0 = 1.494 \pm 0.005$, $R_0 = (100.24 \pm 0.1) h^{-1}\text{Mpc}$.

The only statistically significant differences between D2.75 and C1.2 correlation functions are observed at small radii $R < 5 h^{-1}\text{Mpc}$, which are due to the differences in the force resolution. This indicates that the $1.2 h^{-1}\text{Gpc}$ box of

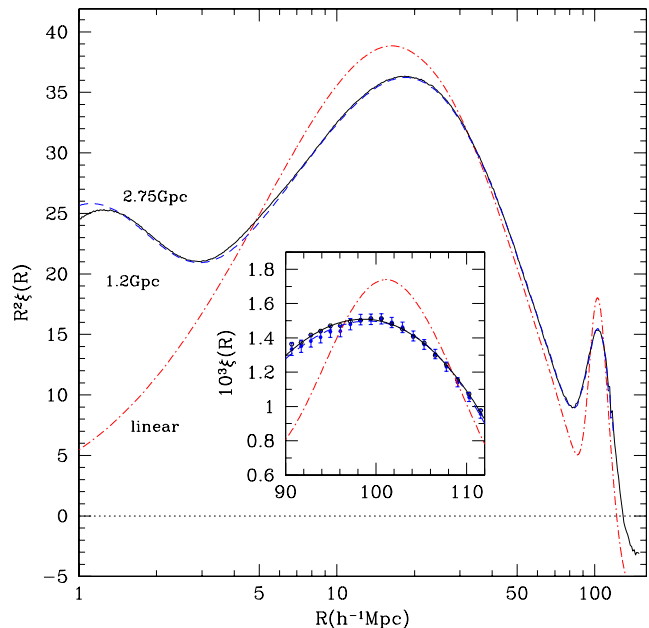


Figure 7. Comparison of nonlinear dark matter correlation functions. Full and dashed curves show the results from the D2.75 and C1.2 GLAM simulations correspondingly. Differences at $R < 5 h^{-1}\text{Mpc}$ radii are explained by the higher resolution of the C1.2 simulations. At larger scales there are no measurable differences between the $L = 1.2 h^{-1}\text{Gpc}$ and the much larger $L = 2.75 h^{-1}\text{Gpc}$ simulation boxes. The insert in the figure shows in more detail the region around the BAO peak. The error bars in the plot correspond to 1σ -errors of the mean as evaluated using the 100 realisations of the C1.2 simulation. Full and dashed curves present analytical fits eq.(8) with differences in the position of the BAO peak less than 0.1%.

the C1.2 simulations is large enough to produce accurate results for the scales presented in Figure 7.

7 DENSITY DISTRIBUTION FUNCTION

The density distribution function of the dark matter $P(\rho)$ provides an additional test for the effects of the finite-box size L . One may expect some impact due to the missing waves. Indeed, a very long wave with a wavelength longer than L increases the *rms* fluctuations inside the computational box. As the result, some fluctuations collapse earlier when the density of the universe is larger. Thus, the collapsed density will be somewhat larger as compared with the situation when the long-wave is missed in simulations with box-size L . Using the same argument, one expects that some regions will have lower density, if the long-wave is present. In other words, the density distribution function should be wider in simulations with larger boxes. This is the same type of arguments that were mentioned in the estimates of the halo abundances: the effect must be present, but how large is it?

Here we will be interested in the high-density tail of $P(\rho)$ because of two reasons: (1) the power spectra and correlation functions – being averages over the whole computational volume – have already gave us results on the prop-

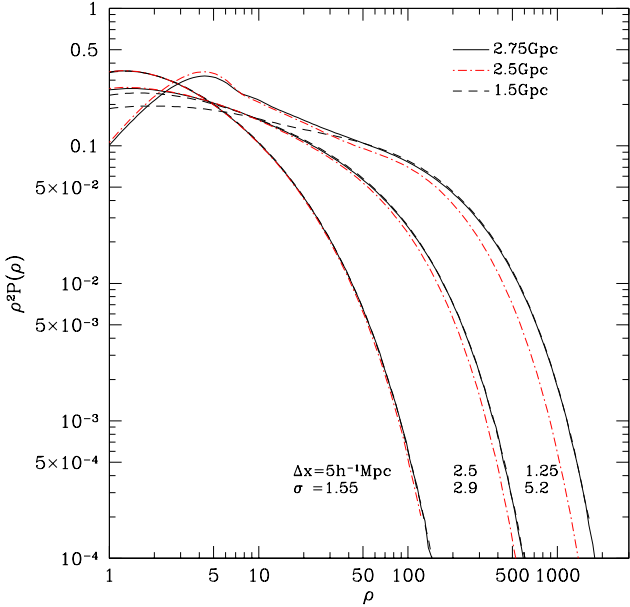


Figure 8. The dark matter density distribution function $P(\rho)$ at $z = 0$ for simulations with different box and cell-sizes. The density is given in the units of the average density of the Universe. The PDF is scaled by the square of density to reduce the dynamical range. The *rms* density fluctuation σ measured for different cell-sizes is indicated in the plot. The lack of force resolution in A2.5 results in the decline of PDF at large densities $\rho > 100$, while the particle noise becomes important for low densities $\rho < 10$. In the regime where both the force and mass resolutions are small the PDF does not show any signs of dependence on the size of simulation box.

erties of the density field. However, they may not be very sensitive to a small fraction of the volume with the largest density; (2) Because of the particle noise in regions with low-density, it is more difficult to reliably estimate the PDF at low ρ .

We select three GLAM simulation sets to study the PDF. The main comparison is between D2.75 and A1.5 with $L = 2.75 h^{-1} \text{Gpc}$ and $L = 1.5 h^{-1} \text{Gpc}$, which have almost two times different box-sizes and the same force resolution. So, the difference between those simulations at large densities should be only due to the box-sizes. However, these simulations have almost ten times different number densities of particles that affects the low-density part of $P(\rho)$. In addition, we also consider the A2.5 simulations that have the same number-density of particles as D2.75, nearly the same volume, but twice lower resolution. The density distribution function $P(\rho)$ is estimated for three filtering scales – sizes of cubic cells: $\Delta x = 1.25, 2.5, 5.0 h^{-1} \text{Mpc}$.

The dark matter density distribution functions $P(\rho)$ are shown in Figure 8. The density is given in the units of the average density of the Universe. The PDF is scaled with the square of density to reduce the dynamical range. The *rms* density fluctuation σ measured for the different cell-sizes is indicated in the plot. For the large cell-size $\Delta x = 5 h^{-1} \text{Mpc}$ the PDFs of the different box sizes are practically indistinguishable. As the cell-size decreases, the lack of the

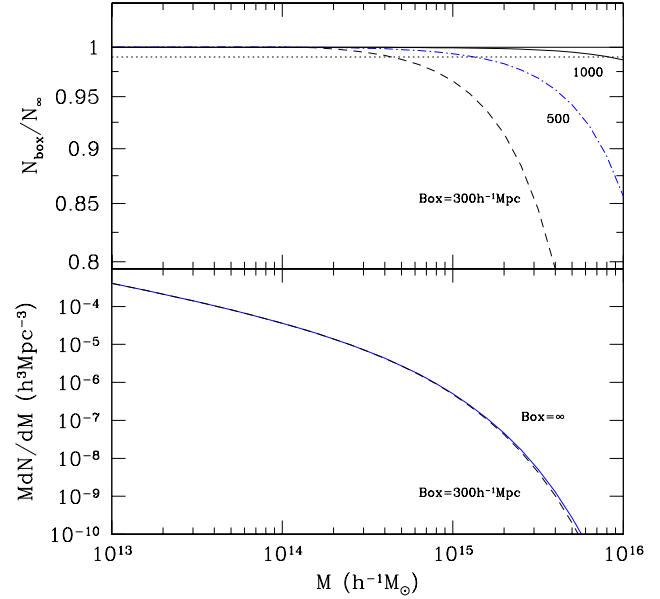


Figure 9. Analytical estimates of the abundance of dark matter halos assuming a truncated linear power spectrum at long waves. The bottom panel shows the halo abundance for a spectrum truncated at the fundamental mode of a $300 h^{-1} \text{Mpc}$ simulation box (dashed curve) as compared to that obtain with an untruncated spectrum (full curve). The top panel shows the ratio of the predicted halo abundances in simulations with different box-sizes to that assuming an untruncated spectrum. The dashed line shows 1% decrease in the halo abundance. There is almost no effect for halos with mass less than $10^{14} h^{-1} M_{\odot}$. The abundance of most massive cluster-size halos with $M \approx 10^{15} h^{-1} M_{\odot}$ can be underestimated by $\sim 5\%$ in simulations with a box-size of $300 h^{-1} \text{Mpc}$, but the effect dramatically decreases with increasing the simulation size and no measurable effect is observed for a $\sim 1 h^{-1} \text{Gpc}$ box.

force resolution in the A2.5 simulations results in the decline of the PDF at large densities $\rho > 100$, while the particle noise becomes important for low densities $\rho < 10$. In the regime where both the force and mass resolutions are small the PDF does not show any signs of dependence on the size of the simulation box.

8 HALO ABUNDANCES

Missing large-scale power in finite box simulations must affect the estimates of the abundance of halos with different masses. All current analytical models – build and tested using N -body results – tell us that halo abundance is a function of the *rms* density fluctuations $\sigma(M, z)$ as estimated from the linear power spectrum smoothed with filter of effective mass M at redshift z . Because the finite box simulations miss some fraction of σ for a given mass M , these simulations must predict fewer halos.

However, so far the results provided by N -body cosmological simulations have failed to show that this is the case (Warren et al. 2006; Tinker et al. 2008; Skillman et al. 2014; Ishiyama et al. 2015; DeRose et al. 2018). The halo mass functions estimated using simulations of different box sizes

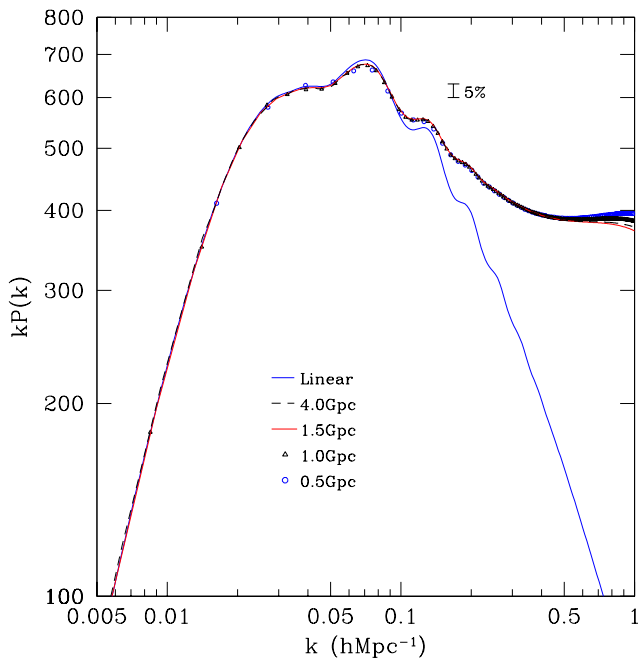


Figure 10. Power spectrum of dark matter fluctuations at $z = 0$ scaled with wavenumber k . Simulations with different computational box-sizes are labeled with different symbols as indicated in the plot. Differences between simulations at large $k \sim 1h\text{Mpc}^{-1}$ are related with the force resolution. On larger scales (small $k < 0.1h\text{Mpc}^{-1}$), where the force resolution is not important, there are no visible signs that the box-size affects the power spectrum.

have been extensively studied in the field. For example, Tinker et al. (2008) used simulations with sizes $L = 80 h^{-1}\text{Mpc}$ up to $L = 1.3 h^{-1}\text{Gpc}$. Skillman et al. (2014) analysed simulations with different box sizes between $100 h^{-1}\text{Mpc}$ and $8 h^{-1}\text{Gpc}$. None of those works indicated any dependance of the halo mass function on the simulation box-size.

In the overlapping halo mass interval $M = 10^{13} - 2 \times 10^{14} h^{-1}M_{\odot}$ the DarkSky simulations with boxes $L = 0.8, 1.6, 8 h^{-1}\text{Gpc}$ have mass functions that deviate by less than 1%. DeRose et al. (2018) do not find any differences in the halo mass function of halos more massive than $\sim 10^{13} h^{-1}M_{\odot}$ when comparing simulations with $1 h^{-1}\text{Gpc}$ and $5 h^{-1}\text{Gpc}$ boxes.

In order to interpret and understand this result we use the analytical approximation of the halo mass function $n(M) = f(\sigma(M, z))$, where $\sigma(M, z)$ is the *rms* of density fluctuations as presented in Comparat et al. (2017). By itself this approximation is based on the MultiDark (Klypin et al. 2016) suite of simulations with box sizes $L = 0.4 - 4 h^{-1}\text{Gpc}$. We use this approximation to find the halo mass function in two ways. First, we estimate the *rms* of fluctuations $\sigma(M, z)$ using the full (untruncated) linear power spectrum of fluctuations. Second, we mimic the finite box-size effects by truncating the power spectrum at the fundamental mode k_{box} .

Figure 9 presents our estimates of the halo mass function for three hypothetical simulations with box sizes $L = 300, 500 h^{-1}\text{Mpc}$ and $1 h^{-1}\text{Gpc}$. Clearly one should expect some deficit of halos in the simulation with $L = 300 h^{-1}\text{Mpc}$. For example, for mass $M = 2 \times 10^{15} h^{-1}M_{\odot}$ the model pre-

dicts that about 10% of the halos will be missed. It is also clear why this effect has not been measured in the N -body simulations, and why it could be ignored: the model predicts that one should find only about one cluster for this halo mass in such small box. Note that when analyzing the simulations, one routinely ignores the first ~ 100 most massive halos because these clusters are too sensitive to cosmic variance and also because of the large statistical errors. If we limit ourselves to a mass scale with more than 100 halos, then the $L = 300 h^{-1}\text{Mpc}$ box yields less than 1% uncertainty in the halo mass function at the most massive tail.

Figure 9 also shows that the finite box-size uncertainties decline dramatically with L . A simulation with a box-size of $1 h^{-1}\text{Gpc}$ will end up with no missing clusters: 1% error is reached for a halo mass of $\sim 8 \times 10^{15} h^{-1}M_{\odot}$. The predicted number of clusters with this mass is so low that no single cluster of this mass is expected in the Universe.

So, when it comes to making a choice for the box-size, our selection depends on the observational sample, i. e. how massive are the clusters in the sample that will be analyzed. For example, if the observed volume is relatively small and we are focusing only on clusters with mass less than $10^{14} h^{-1}M_{\odot}$ then even a $300 h^{-1}\text{Mpc}$ box-size would be sufficient: on average it will produce the correct amount of clusters under consideration. If instead we deal with a very large survey and study all possible clusters, then the box-size must be not less than $1 h^{-1}\text{Gpc}$.

The errorbars in the observed number of objects, which we estimate using simulations, are the sum of two factors: (1) the statistical fluctuations due to the cosmic variance (random noise due to all harmonics with wavelength less than L) and (2) the effects of waves longer than the computational box. The first term will be found by measuring the statistics of objects in many realizations of simulated boxes.

The second term can be estimated by assuming that the number of objects $n(M)$ depends on the *rms* of density fluctuations at a given scale $\sigma(M, z)$. We use the halo mass function as an example. The number of missed halos $\Delta n(M)$ due to change in σ can be written as

$$\frac{\Delta n}{n} = \frac{\partial \ln n(\sigma)}{\partial \sigma} \Delta \sigma, \quad (9)$$

where $\Delta \sigma = \sigma_{\text{miss}}(L)$ is the *rms* fluctuations due to waves longer than L . Note that this is exactly the quantity that is plotted in the top panel of Figure 9. The errors can be substantial for $\sim 10^{15} h^{-1}M_{\odot}$ clusters in $300 h^{-1}\text{Mpc}$ simulations, but they are negligible for any clusters in $1 h^{-1}\text{Gpc}$ runs.

9 FINITE-BOX EFFECTS ON THE POWER SPECTRUM

The accuracy of the non-linear dark matter power spectrum from N -body simulations has been addressed extensively in many publications (e.g., Heitmann et al. 2008, 2010; Schneider et al. 2016; Lawrence et al. 2017; Smith & Angulo 2018). However, typically the main focus of these works is devoted to the convergence of the results on the short-scales (see also Smith & Angulo (2018)). Unlike the short scales, where the comparison of just one or few realisations with different box-sizes is sufficient, the analysis of the power spectrum

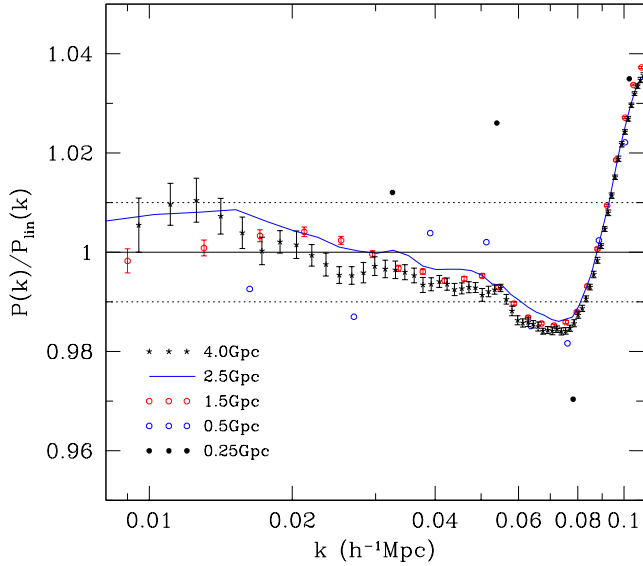


Figure 11. The ratio of the non-linear to linear power spectrum – square of the bias parameter – for simulations with different box-sizes. The bias parameter is scale dependent on $k \gtrsim 0.05 h\text{Mpc}^{-1}$. To avoid clutter we show statistical errors only for D4.0 and C1.5 simulations. Because of the small number of realizations the $4 h^{-1}\text{Gpc}$ simulations show relatively large noise. Small-box simulations (D0.25 and D0.5) have $\sim 2\%$ deviations from the average trend due to noise. Simulations with box sizes $> 1 h^{-1}\text{Gpc}$ do not indicate a trend with the box-size.

for long-waves ($k \lesssim 0.3 h\text{Mpc}^{-1}$) is complicated due to the large cosmic variance, which would require many realisations in order to complete a detailed study. Heitmann et al. (2010) compared the power spectrum results obtained with $234 h^{-1}\text{Mpc}$, $960 h^{-1}\text{Mpc}$ and $2 h^{-1}\text{Gpc}$ simulation boxes. They find that the power spectrum of 137 realisations of the $234 h^{-1}\text{Mpc}$ boxes is below the larger box simulations by about $\sim 1\%$ for wavenumbers $k = 0.03 - 0.15 h\text{Mpc}^{-1}$. There were no detectable differences (less than $\sim 1\%$ between their $960 h^{-1}\text{Mpc}$ and $2 h^{-1}\text{Gpc}$ boxes). Klypin & Prada (2018) used thousands of realisations to study the effects of the simulation box-size on the average of the power spectrum. Here, we extend that analysis to study in detail the effects of longer waves with additional simulations.

Similar to the situation with the halo abundance, we know how qualitatively the missed long waves affect the power spectrum: power spectrum must increase with increasing of the box size. The magnitude of the effect is difficult to estimate. However, we know that the missing power is small for any realistic box-size (see Figure 4). Thus, most of the effect is expected to be found on long-waves in a given computational box. However, these waves are still in nearly linear regime and their non-linear coupling with the small amplitude waves outside the box can be expected to be small.

The average power spectra obtained from the different sets of simulations are shown in Figure 10. The only differences one can see in this plot are those due to the force

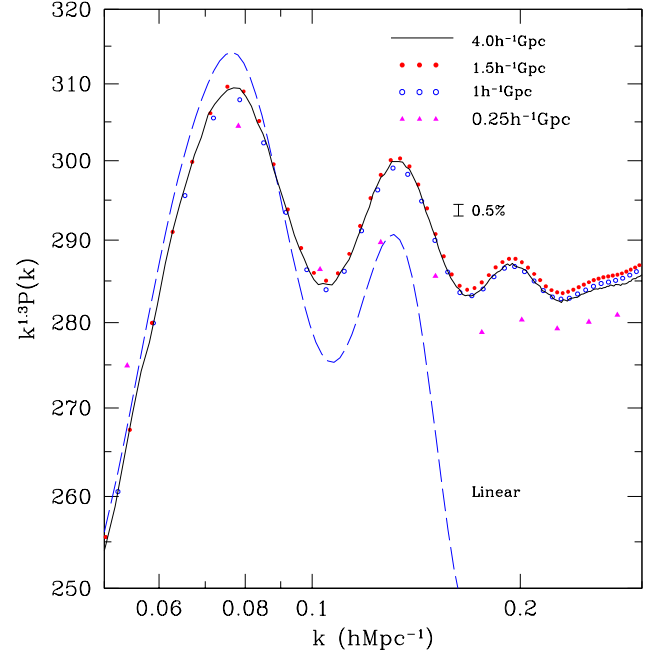


Figure 12. Power spectra of dark matter in the domain of BAO peaks. The spectra are scaled with a $k^{1.3}$ factor to reduce the dynamical range. The vertical bar in the plot corresponds to $1/2$ of percent deviations. The large-box simulations with $L \gtrsim 1 h^{-1}\text{Gpc}$ show remarkable degree of convergence with the differences less than $\sim 0.1\%$. The small-box simulations D0.25 systematically fall below the rest by $\sim 1 - 1.5\%$.

resolution: increasing resolution in small-box simulations results in the increase of the amplitude of the power spectrum. This happens at large wavenumbers $k \gtrsim 0.5 h\text{Mpc}^{-1}$, which is a clear signature of the resolution effects. The finite-box effects should act in the opposite direction by decreasing the power in small-boxes relative to the bigger ones. There are no obvious signs of the box-size effects on long-waves where one expects them to be present.

In order to see the effects on small wavenumbers more clearly, we plot the ratio of the nonlinear power spectrum to the linear spectrum $P(k)/P_{\text{linear}}(k)$ – the square of the bias parameter. The results presented in Figure 11 do not show any signatures of depression in the power spectrum due to the missing long-waves. The outliers in this panel are coming from the small $L = 250 h^{-1}\text{Mpc}$ and $L = 500 h^{-1}\text{Mpc}$ simulations. There may exist a small effect of the box-size at $k = (0.01 - 0.02) h\text{Mpc}^{-1}$ where the bias systematically increases by $\sim 0.5\%$ with increasing box-size, but the deviations are within the statistical uncertainties due to the small number of realisations of the $4.0 h^{-1}\text{Gpc}$ box.

One effect is nevertheless noticeable: the large spacing between points for small-box simulations. This is related with the fundamental harmonic k_{box} that defines discreteness effects in the Fourier space (minimum separation of harmonics): the larger is the box, the smaller is the binning. This can be a serious problem for small boxes. For example, for $L = 250 h^{-1}\text{Mpc}$ the minimum width of a bin Δk is $\Delta k = 0.025 h\text{Mpc}^{-1}$, which should be compared with the wavenumber of the first BAO peak $\sim 0.07 h\text{Mpc}^{-1}$. So, the binning is smaller than the BAO wavenumber, but only ~ 3

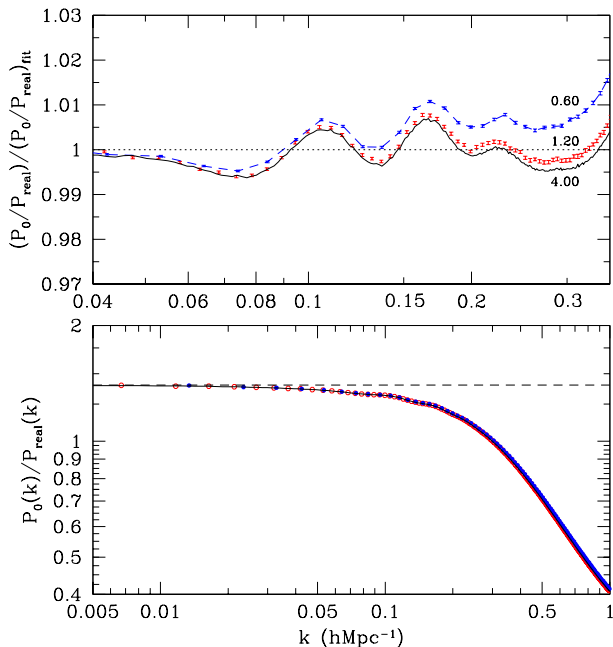


Figure 13. Redshift distortions in simulations with different box sizes. Full curves show results for D4 simulations with 4 Gpc box. These are compared with results for much smaller simulations with $1.2 h^{-1}\text{Gpc}$ and $600 h^{-1}\text{Mpc}$ box sizes. *The bottom panel:* ratio of the redshift-space dipole power spectrum P_0 to the real-space P_{real} . The horizontal dashed line indicates theoretical prediction for very long waves (Kaiser 1987). Open (red) and filled circles (blue) are for simulations with the same mass and force resolution as D4 but in $1.2 h^{-1}\text{Gpc}$ and $600 h^{-1}\text{Mpc}$ boxes correspondingly. *The top panel:* Deviations P_0/P_{real} ratios from a smooth analytical function eq.(10). Differences between 4 Gpc and 1.2 Gpc are very small $\lesssim 0.1\%$ at all scales. Decreasing the box size to $600 h^{-1}\text{Mpc}$ results in $\sim 1\%$ errors at $k \gtrsim 0.2 h\text{Mpc}^{-1}$ and no measurable errors at very long waves $k \lesssim 0.05 h\text{Mpc}^{-1}$.

times. Indeed, the points in Figure 11 that deviate from the other estimates of the $P(k)/P_{\text{linear}}(k)$ ratio are those that correspond to the small $L = 250 h^{-1}\text{Mpc}$ simulations.

Figure 12 presents a zoom-in view on the BAO domain of the power spectrum. We multiply the power spectrum $P(k)$ by factor $k^{1.3}$ with the goal to flatten the curves in the range $k = (0.1 - 0.3)h\text{Mpc}^{-1}$. Simulations D0.25 with small box sizes clearly suffer from the lack of long-waves: their power spectrum is systematically fall below the rest by $\sim 1 - 1.5\%$. This is consistent with estimates of Heitmann et al. (2010). There are no measurable deviations between $1 h^{-1}\text{Gpc}$ and $4 h^{-1}\text{Gpc}$ simulation boxes with differences less than $\sim 0.1\%$.

Presented results so far were done for quantities defined in real space and did not include peculiar velocities. The latter produce distortions in the redshifts space that are important component of the interpreting and understanding of observed clustering of objects (e.g., Kaiser 1987; Hamilton 1998; Reid & White 2011; Sánchez et al. 2017). Because our results are based on N -body simulations where density and velocity perturbations play equally important roles, accurate estimates of the growth and evolution of density fluctuations imply accurate estimates of peculiar velocities. In

other words, convergence of different statistics of density distribution guarantees convergence of quantities in redshift space. To make this argument more clear, we compare redshift space power spectra with those done in the real space.

When estimating the redshift-space power spectra, we perturb positions of particles along one of coordinate axes according to their peculiar velocities and periodically wrap them around, if necessary. Once the density in the redshift space is constructed, we find the spectrum and estimate either the monopole or quadrupole power spectrum. Results are averaged over three directions of velocity distortions.

We use 100 realizations of the D4 simulations to make estimates of power spectra for large-box simulations. To find effects of the box size we additionally made 100 realizations with a $1.2 h^{-1}\text{Gpc}$ box-size and 800 realizations with twice smaller $600 h^{-1}\text{Mpc}$ boxes. For these simulations we use exactly the same mass and force resolution as for the D4 simulations: 600^3 particles moving in a 1200^3 mesh for $1.2 h^{-1}\text{Gpc}$ simulations and 300^3 particles moving in a 600^3 mesh for $600 h^{-1}\text{Gpc}$ simulations. Because we are interested only in the effects of peculiar velocities, we analyze the ratios of the redshift to real-space power spectra. This greatly reduces the cosmic variance and allows us to dramatically reduce the statistical noise.

Figure 13 presents results for the monopole component (quadrupole component shows similar results). Full curves show results for the $4 h^{-1}\text{Gpc}$ box. Different symbols are for the $600 h^{-1}\text{Mpc}$ and $1.2 h^{-1}\text{Gpc}$ boxes. The bottom panel shows the ratio of the redshift-space dipole power spectrum P_0 to the real-space P_{real} . The horizontal dashed line indicates theoretical prediction for very long waves (Kaiser 1987): $P_0 = (1 + 2f/3 + f^2/5)P_{\text{real}}$, where $f = d \ln \Delta / d \ln a$ is the grows rate of linear waves (e.g., Reid & White 2011). Differences between simulations with different box sizes are so small that it is difficult to see them. To find the differences, we fit the ratio P_0/P_{real} with an analytical smooth function and display the deviations from the same fit in the top panel. The function itself is motivated by approximations used in the field. Specifically we use analytical approximation:

$$\left(\frac{P_0}{P_{\text{real}}}\right)_{\text{fit}} = A \exp \left[- \left(\frac{k}{k_0} \right) - \left(\frac{k}{k_1} \right)^2 \right], \quad (10)$$

where $A = 1.40$, $k_0 = 2.4 h\text{Mpc}^{-1}$, and $k_1 = 0.66 h\text{Mpc}^{-1}$. The differences between $4 h^{-1}\text{Gpc}$ and $1.2 h^{-1}\text{Gpc}$ simulations are small: less than $\sim 0.1\%$ on all scales. At even smaller $L = 600 h^{-1}\text{Mpc}$ simulations show some differences at $k \gtrsim 0.1 h\text{Mpc}^{-1}$. However, they are relatively small (e.g., $\sim 1\%$ at $k \gtrsim 0.2 h\text{Mpc}^{-1}$). There are no measurable difference at very long waves with $k \lesssim 0.05 h\text{Mpc}^{-1}$.¹

¹ The limited force resolution $\epsilon = 1 h^{-1}\text{Mpc}$ for the $4 h^{-1}\text{Gpc}$ box and for smaller boxes used for Figure 13 affect (underestimate) the redshift distortions at large wavenumbers $k \gtrsim 0.2 h\text{Mpc}^{-1}$. For a much better resolution of $\epsilon = 0.25 h^{-1}\text{Mpc}$ and box size $L = 1 h^{-1}\text{Gpc}$ we find that parameters are slightly different: $A = 1.405$, $k_0 = 1.84 h\text{Mpc}^{-1}$, and $k_1 = 0.55 h\text{Mpc}^{-1}$. This approximation gives errors less than 0.5% for $k < 0.35 h\text{Mpc}^{-1}$.

10 COVARIANCE MATRIX OF THE POWER SPECTRUM

The covariance matrix $C(k, k')$ of the power spectrum given in eq.(2) is one of the main statistics required for detailed analysis of observational survey data and estimates of cosmological parameters (see e.g., Anderson et al. 2012; Sánchez et al. 2012; Dodelson & Schneider 2013; Percival et al. 2014). It is very difficult to estimate the covariance matrix using simulations because thousands of realisations are required in order to produce accurate measurements (e.g., Taylor et al. 2013; Percival et al. 2014; Klypin & Prada 2018). This is also a quantity that strongly depends on the computational box-size. So, it is important to understand how to handle $C(k, k')$ obtained from finite-volume simulations (e.g., Gnedin et al. 2011; Li et al. 2014a; Mohammed & Seljak 2014; Bertolini et al. 2016).

The diagonal and off-diagonal components of the covariance matrix have different nature and different magnitudes. The diagonal components $C(k, k)$ are defined mostly by the Gaussian noise associated with the finite number of Fourier harmonics found in each bin used to estimate the power spectrum. As such, we can write:

$$C^G(k, k) = \alpha \frac{2}{N_h} P^2(k), \quad N_h = \frac{4\pi k^2 \Delta k}{(2\pi/L)^3}, \quad (11)$$

where N_h is the number of harmonics in a $[k, k + \Delta k]$ bin and the coefficient α takes into account the filtering due to the binning process. For the Near Grid Point (NGP) binning $\alpha = 1$, and $2/3$ for the CIC binning. Note that the magnitude of the diagonal components is proportional to the volume of the simulations, i. e.,

$$Cov(k, k) \propto L^{-3}. \quad (12)$$

Nonlinear clustering affects the diagonal components at large wavenumbers ($k \gtrsim 0.2 h \text{Mpc}^{-1}$) making them larger than the simple shot-noise estimates. However, the nonlinear terms also scale with volume (Klypin & Prada 2018).

The non-diagonal components $C(k, k')$ have much smaller amplitudes but there are many more of them as compared with the diagonal ones. So, the off-diagonal components are still important. Detailed analysis of these components was presented in Klypin & Prada (2018) who found that they also scale with the computational volume. Here we present a couple of examples of the behaviour of the covariance matrix in the domain of the BAO peaks.

Figure 14 presents two slices of the dark matter covariance matrices $Cov(k, k')$ in simulations with different box sizes. All covariance matrices were rescaled to the $1.5 h^{-1} \text{Gpc}$ box-size by multiplying $Cov(k, k')$ by the ratio of volumes. The covariance matrix of the $2.5 h^{-1} \text{Gpc}$ simulations (A2.5c) was additionally scaled up by 10%. Without this re-scalings the difference between the covariance matrices is very large: factor $(2.5/0.96)^3 \approx 18$ between simulations with $2.5 h^{-1} \text{Gpc}$ and $1 h^{-1} \text{Gpc}$. The large level of noise of the covariance matrix for the $2.5 h^{-1} \text{Gpc}$ simulations is due to the fact that the level of the signal is very low due to the large box-size.

These results make the rescaling of the covariance matrices easy: one can rescale the covariance matrix proportionally to the ratio of the volumes. In the next section we will discuss in detail the covariance corrections due to super sample modes.

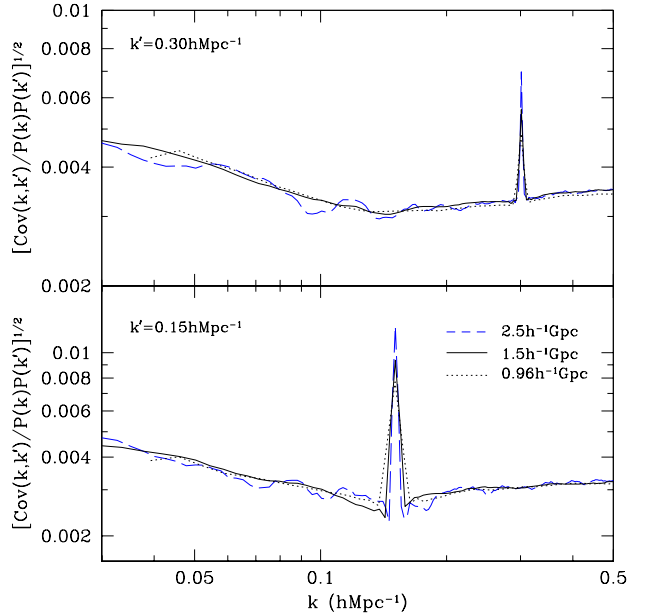


Figure 14. Two slices of the dark matter covariance matrices $Cov(k, k')$ in simulations with different box sizes as indicate the labels in the bottom panel. All covariance matrices were rescaled to $1.5 h^{-1} \text{Gpc}$ box-size by multiplying $Cov(k, k')$ by the ratio of volumes. Without this re-scaling the difference between the covariance matrices is very large.

11 SUPER SAMPLE COVARIANCE

In this paper we have addressed so far the impact of missing long-waves by studying the scaling of different quantities such as correlation function, PDF, halo abundance, power spectrum, and covariance matrix with the box-size. As the box-size increases, more and more long-waves are incorporated into the simulations. The extrapolation of these quantities to the limit of infinitely large boxes gives us the estimates of those true quantities. These convergence studies are the traditional way of treating situations like that. This would work if the observational sample is very large and we measure a fair volume fraction of the Universe. Indeed, the current and future galaxy surveys have very large volumes. For example, the effective volume of DESI or Euclid will be $\sim 50 h^{-1} \text{Gpc}^3$, which roughly corresponds to the volume of a simulation box with $L \sim 3.7 h^{-1} \text{Gpc}$.

There is another approach to the problem of waves longer than the observed sample or computational volume that aims to estimate their effects using a simplified model. The key assumption of this approach is that waves that are longer than L can be considered to have a constant (background) density δ_b inside the simulation box (see e.g. Baldauf et al. 2011; Takada & Hu 2013; Li et al. 2014b; Baldauf et al. 2016). These very long-waves affect the growth of fluctuations inside a given box L that is extracted from a density field that does not have any missing long-waves. There is an obvious question regarding the accuracy of the approximation: as we saw in Section 5 most of the missing power is in waves that are only twice longer than the box-size L , and, thus cannot be considered to be constant inside the computational box. Let's ignore for now this question and see what

the *Super Scale Covariance* (SSC) approach predicts for the covariance matrix.

The covariance matrix can be written as a sum of three terms: the Gaussian contribution given by eq.(11), the non-linear term related with the tri-spectrum of perturbations, and the contribution of waves longer than L :

$$Cov_{ij} = Cov^G(k_i, k_j)\delta_{ij} + Cov^T(k_i, k_j) + Cov^{SSC}(k_i, k_j). \quad (13)$$

The first two terms scale with the volume of the simulation $Cov^{G,T} \propto L^{-3}$ as discussed in Section 10. These two terms are estimated from finite-box simulations. For this reason we combine these two terms together and refer to the sum as Cov_{ij}^{Box} .

The SSC term is due to the response of the power spectrum $P(k)$ to the background density change δ_b in the box L , i. e., $\delta P(k) = (dP(k)/d\delta_b)\delta_b$. Averaging over the distribution of δ_b gives an estimate of the SSC covariance term (Takada & Hu 2013; Li et al. 2014a; Wagner et al. 2015):

$$Cov_{ij}^{SSC} \approx \sigma_L^2 \frac{\partial \ln P_i}{\partial \delta_b} \frac{\partial \ln P_j}{\partial \delta_b} P_i P_j, \quad (14)$$

where σ_L is the *rms* of δ_b as measured in boxes of size L . On large scales (small k) the response function $d \ln P(k)/d\delta_b$ changes relatively slowly (e.g., Takada & Hu 2013; Li et al. 2014b; Mohammed et al. 2017), and its magnitude depends on how the power spectrum is measured. If $P(k)$ is measured with respect to the local density of the simulation box $1 + \delta_b$ then the effect is substantially smaller as compared with that when the clustering is relative to the true background density. For large galaxy surveys the clustering is relative to the average density of the galaxy sample in the observed volume. To mimic the observations we can always mimic the same in our simulations.

In the limit of small k the response function can be written as (e.g., Mohammed et al. 2017):

$$\frac{\partial \ln P}{\partial \delta_b} = \frac{5}{21} - \frac{1}{3} \frac{d \ln P}{d \ln k} \approx 0.57; \quad (15)$$

where this estimate is given for the power spectrum with slope -1, which is the typical value for the long-waves $k = (0.1 - 0.3)h\text{Mpc}^{-1}$. Note that if the overall density is used for the background, then the first factor $5/21$ in eq. 15 should be replaced with $41/21$ and the response function will value ≈ 2.3 .

We estimate the *rms* of δ_b fluctuations using a series of $4 h^{-1}\text{Gpc}$ GLAM simulations with 1500^3 particles and 3000^3 mesh. Each simulation was split in either $500 h^{-1}\text{Mpc}$ or $1 h^{-1}\text{Gpc}$ sub-boxes, and the total density of each sub-box was used to find σ_L . As expected, the results are accurately fitted by a power-law with the slope -2:

$$\sigma_L = \frac{1.43 \times 10^{-3}}{L_{\text{Gpc}}^2}, \quad L_{\text{Gpc}} \equiv \frac{L}{1 h^{-1}\text{Gpc}} \quad (16)$$

Now we estimate the impact of SSC covariance term on the normalized covariance matrix, i. e.,

$$\frac{C_{ij}}{P_i P_j} = \frac{C_{ij}^{\text{Box}}}{P_i P_j} + \sigma_L^2 \frac{\partial \ln P_i}{\partial \delta_b} \frac{\partial \ln P_j}{\partial \delta_b} \quad (17)$$

$$\approx \frac{C_{ij}^{\text{Gpc}}}{P_i P_j} \frac{1}{L_{\text{Gpc}}^3} + \left[\frac{0.0285}{L_{\text{Gpc}}} \right]^4, \quad (18)$$

where C_{ij}^{Gpc} is the box covariance matrix measured for $L = 1 h^{-1}\text{Gpc}$ and L_{Gpc} is the box size in units $h^{-1}\text{Gpc}$.

This relation can be used to estimate the correction to the covariance matrix in simulations with a given box-size due to the super-sample modes. For example, the covariance matrix estimated for $L = 1.5 h^{-1}\text{Gpc}$ in Figure 14 is $[Cov_{ij}/P_i P_j]^{1/2} \approx (3 - 4) \times 10^{-3}$ for non-diagonal components in a wide range of wavenumbers $0.05 h\text{Mpc}^{-1} < k < 0.5 h\text{Mpc}^{-1}$. Thus, for these simulations the covariance matrix corrected by the SSC terms is given by

$$\left[\frac{Cov_{ij}^{\text{correct}}}{P_i P_j} \right]^{1/2} = \left[\frac{Cov_{ij}^{\text{Box}}}{P_i P_j} \right]^{1/2} [1 + (4 - 7) \times 10^{-3}]. \quad (19)$$

The correction is about 0.5%, which is small, but can be relevant for some very sensitive applications. The estimate for $4 h^{-1}\text{Gpc}$ simulations shows a 0.2% correction.

The situation becomes totally different if the true background density is used for the power spectrum estimates of a small computation box. For example, a box with $L = 500 h^{-1}\text{Mpc}$ is often used in the literature for SSC estimates (e.g., Li et al. 2014a; Wagner et al. 2015; Mohammed et al. 2017). In this case the covariance matrix is dominated by the super-sample modes. Indeed, for this case our estimates show that $[Cov_{ij}/P_i P_j]^{1/2}$ almost doubles due to the SSC corrections.

So, SSC corrections can be quite important for surveys with small volumes or for simulations with small box size. However, they are small for studies of galaxy clustering statistics with effective volumes of tens of Gpc^3 .

12 CONCLUSIONS AND SUMMARY

Modern galaxy surveys encompass larger volume of space prompting the theory to make a careful analysis of the effects of very long waves on the observable statistics such as the power spectrum, the correlation functions, PDF, covariances, and the abundances of rich clusters of galaxies. Cosmological simulations play a key role in this analysis. It is routinely assumed that a single cosmological simulation box must cover the volume of the whole observable catalog. This significantly complicates the theoretical analysis and makes nearly impossible to perform thousands of realizations of mock galaxy samples required for estimates of systematics and errors. We challenge this trend and make extensive analysis of the effects due to the finite box-size of the cosmological simulations.

We argue that for most of the types of analysis of large-scale surveys a computational volume of $L \sim (1 - 1.5) h^{-1}\text{Gpc}$ is sufficient. In order to produce mock observed catalogs, these finite-volume simulations should be periodically replicated to fill the required observational volume. We also show that no corrections are required to the average power spectrum and correlation function, PDF and halo abundances, due to the effect of missing long-waves in a simulation box. On the other hand, the covariance matrices should be scaled down proportionally to the volume of the observations and, if necessary, corrected for the super-sample modes as given in eq.(12) and eq.(18).

Here is the summary of our main results:

– Defects of box replications can be readily remedied by a combination of sufficiently large $\sim 1 h^{-1}\text{Gpc}$ simulations

and rotation of the boxes before building mock galaxy catalogs,

- The missing power of finite-box simulations (due to waves longer than the computational box) dramatically declines with increasing box-size L , and becomes extremely small $\sigma \lesssim 0.01$ for $L \gtrsim 1 h^{-1}\text{Gpc}$. Most of the missing power is in waves that are slightly longer than the box-size: about 90% of the missing power is in waves with wavelengths $(1 - 1.5)L$,

- Corrections to the abundance of halos and galaxies are extremely small and can be neglected for computational volumes larger than $1 h^{-1}\text{Gpc}$,

- The average power spectra of dark matter fluctuations show remarkable lack of dependence on the size of the computational box. We clearly detect some decline of the amplitude of fluctuations for small $(250 - 500) h^{-1}\text{Mpc}$ boxes, but it is small: $(1 - 1.5)\%$ for the smallest $250 h^{-1}\text{Mpc}$ simulation that we studied. There are no visible effects for simulations with $L > 1 h^{-1}\text{Gpc}$ with upper limits of $\sim 0.5\%$ for extremely long-waves with $k = (0.008 - 0.05)h\text{Mpc}^{-1}$ and less than $\sim 0.1\%$ for waves in the BAO domain with $k = (0.07 - 0.3)h\text{Mpc}^{-1}$.

- The covariance matrix of the dark matter power spectra scales proportionally to the computational volume. This well known result (e.g., Takada & Hu 2013; Wagner et al. 2015; Klypin & Prada 2018) is important for using mock galaxy catalogs: the covariance matrix must be scaled down to match the observational sample. The SSC correction to the covariance matrix is expected to be $\sim 0.5\%$ for observational samples with effective volume $3(h^{-1}\text{Gpc})^3$ (box-size $L = 1.5 h^{-1}\text{Gpc}$), and becomes negligible when the observational sample increases to $\sim 50(h^{-1}\text{Gpc})^3$ expected for DESI/Euclid and LSST surveys.

- The most stringent constraints on the simulation volume are coming from the requirement that mock catalogs should reproduce not only the correct power spectra, but also the correlation functions (Sirko 2005; Klypin et al. 2013). We find that the correlation functions for $L \lesssim 500 h^{-1}\text{Mpc}$ are qualitatively incorrect. For example, for $L = 500 h^{-1}\text{Mpc}$ the dark matter correlation function is zero at $R \approx 85 h^{-1}\text{Mpc}$ where it must be positive. For $L = 300 h^{-1}\text{Mpc}$ the correlation function is negative for the whole domain of the BAO peak ($R \approx 100 h^{-1}\text{Mpc}$). However, the effect quickly becomes very small with increasing volume and is negligible for $L \gtrsim 1 h^{-1}\text{Gpc}$.

Based on the work presented in this paper we conclude that a simulation box of $L \sim (1 - 1.5) h^{-1}\text{Gpc}$ is large enough to fulfil most of the science requirements, in the fields of large-scale structure, weak-lensing and cosmological parameters, of the upcoming new generation of large redshift surveys.

ACKNOWLEDGEMENTS

We thank J. Peacock and M. Schmittfull for discussions and comments. A.K. acknowledges support of the Fulbright Foundation, support of the Instituto de Astrofísica de Canarias, La Laguna, and the Severo Ochoa scholarship. A.K. and F.P. acknowledges support from the Spanish MINECO

grant AYA2014-60641-C2-1-P. F.P. wants to thank the support and hospitality of the ICC at Durham University where part of this work was completed. The new GLAM simulations presented in this paper were done at the Barcelona Supercomputer Center (Spain) and the DiRAC Data Centric system at Durham University, operated by ICC on behalf of the STFC DiRAC HPC Facility. We thank New Mexico State University (USA) and Instituto de Astrofísica de Andalucía CSIC (Spain) for hosting the skiesanduniverse.org site for cosmological simulation products.

REFERENCES

- Alam S. et al., 2017, MNRAS, 470, 2617
 Anderson L. et al., 2012, MNRAS, 427, 3435
 Angulo R. E., White S. D. M., 2010, MNRAS, 405, 143
 Baldauf T., Seljak U., Senatore L., Zaldarriaga M., 2011, JCAP, 10, 031
 Baldauf T., Seljak U., Senatore L., Zaldarriaga M., 2016, JCAP, 9, 007
 Bertolini D., Schutz K., Solon M. P., Walsh J. R., Zurek K. M., 2016, Phys. Rev. D, 93, 123505
 Bouchet F. R., Schaeffer R., Davis M., 1991, ApJ, 383, 19
 Cole S., 1997, MNRAS, 286, 38
 Comparat J., Prada F., Yepes G., Klypin A., 2017, MNRAS, 469, 4157
 Dawson K. S. et al., 2016, AJ, 151, 44
 DeRose J. et al., 2018, ArXiv e-prints
 DESI Collaboration et al., 2016, ArXiv e-prints
 Dodelson S., Schneider M. D., 2013, Phys. Rev. D, 88, 063537
 Eisenstein D. J. et al., 2005, ApJ, 633, 560
 Gnedin N. Y., Kravtsov A. V., Rudd D. H., 2011, Rev. Astrn. Astrophys., 194, 46
 Habib S. et al., 2016, New Astronomy, 42, 49
 Hamilton A. J. S., 1998, in Hamilton D., ed., Astrophysics and Space Science Library Vol. 231, The Evolving Universe. p. 185
 Hawkins E. et al., 2003, MNRAS, 346, 78
 Heitmann K. et al., 2008, Computational Science and Discovery, 1, 015003
 Heitmann K., White M., Wagner C., Habib S., Higdon D., 2010, ApJ, 715, 104
 Hu W., Kravtsov A. V., 2003, ApJ, 584, 702
 Ishiyama T., Enoki M., Kobayashi M. A. R., Makiya R., Nagashima M., Oogi T., 2015, PASJ, 67, 61
 Jenkins A. et al., 1998, ApJ, 499, 20
 Kaiser N., 1987, MNRAS, 227, 1
 Klypin A., Prada F., 2018, MNRAS, 478, 4602
 Klypin A., Prada F., Betancort-Rijo J., Albareti F. D., 2017, ArXiv e-prints
 Klypin A., Prada F., Yepes G., Hess S., Gottlöber S., 2013, ArXiv e-prints
 Klypin A., Primack J., Holtzman J., 1996, ApJ, 466, 13
 Klypin A., Yepes G., Gottlöber S., Prada F., Heß S., 2016, MNRAS, 457, 4340
 Laureijs R. et al., 2011, ArXiv e-prints
 Lawrence E. et al., 2017, ApJ, 847, 50
 Li Y., Hu W., Takada M., 2014a, Phys. Rev. D, 89, 083519
 Li Y., Hu W., Takada M., 2014b, Phys. Rev. D, 90, 103530
 LSST Science Collaboration et al., 2009, ArXiv e-prints

- Mohammed I., Seljak U., 2014, MNRAS, 445, 3382
Mohammed I., Seljak U., Vlah Z., 2017, MNRAS, 466, 780
Percival W. J. et al., 2014, MNRAS, 439, 2531
Potter D., Stadel J., Teyssier R., 2017, Computational Astrophysics and Cosmology, 4, 2
Reid B. A., White M., 2011, MNRAS, 417, 1913
Sánchez A. G. et al., 2017, MNRAS, 464, 1640
Sánchez A. G. et al., 2012, MNRAS, 425, 415
Schneider A. et al., 2016, JCAP, 4, 047
Sirko E., 2005, ApJ, 634, 728
Skillman S. W., Warren M. S., Turk M. J., Wechsler R. H., Holz D. E., Sutter P. M., 2014, ArXiv e-prints
Smith R. E., Angulo R. E., 2018, ArXiv e-prints
Spergel D. et al., 2013, ArXiv e-prints
Springel V., 2005, MNRAS, 364, 1105
Takada M., Hu W., 2013, Phys. Rev. D, 87, 123504
Taylor A., Joachimi B., Kitching T., 2013, MNRAS, 432, 1928
Tinker J., Kravtsov A. V., Klypin A., Abazajian K., Warren M., Yepes G., Gottlöber S., Holz D. E., 2008, ApJ, 688, 709
Tormen G., Bertschinger E., 1996, ApJ, 472, 14
Wagner C., Schmidt F., Chiang C.-T., Komatsu E., 2015, MNRAS, 448, L11
Warren M. S., Abazajian K., Holz D. E., Teodoro L., 2006, ApJ, 646, 881